

*Journal of*  
***Mechanics of***  
***Materials and Structures***

**INVESTIGATION OF MODE II CRACK GROWTH FOLLOWING A  
VERY HIGH SPEED IMPACT**

Wei Ma and Zhuping Duan

***Volume 3, N° 2***

***February 2008***



mathematical sciences publishers

## INVESTIGATION OF MODE II CRACK GROWTH FOLLOWING A VERY HIGH SPEED IMPACT

WEI MA AND ZHUPING DUAN

A recoverable plate impact testing technology has been developed for studying fracture mechanisms of mode II crack. With this technology, a single duration stress pulse with submicrosecond duration and high loading rates, up to  $10^8 \text{ MPa m}^{1/2}\text{s}^{-1}$ , can be produced. Dynamic failure tests of Hard-C 60# steel were carried out under asymmetrical impacting conditions with short stress-pulse loading. Experimental results show that the nucleation and growth of several microcracks ahead of the crack tip, and the interactions between them, induce unsteady crack growth. Failure mode transitions during crack growth, both from mode I crack to mode II and from brittle to ductile fracture, were observed. Based on experimental observations, a discontinuous crack growth model was established. Analysis of the crack growth mechanisms using our model shows that the shear crack extension is unsteady when the extending speed is between the Rayleigh wave speed  $c_R$  and the shear wave speed  $c_s$ . However, when the crack advancing speed is beyond  $c_s$ , the crack grows at a steady intersonic speed approaching  $\sqrt{2}c_s$ . It also shows that the transient mechanisms, such as nucleation, growth, interaction and coalescence among microcracks, make the main crack speed jump from subsonic to intersonic and the steady growth of all the subcracks causes the main crack to grow at a stable intersonic speed.

### 1. Introduction

During the past several decades, researchers have made great progress in experiments on dynamic failure mechanisms [Erdogan and Sih 1963; Kalthoff 1987; 1988; Ravichandran and Clifton 1989; Kalthoff 1990; Prakash and Clifton 1992; Ravi-Chandar 1995; Zhou et al. 1996; Needleman 1999; Rosakis et al. 1999; Abraham and Gao 2000; Ravi-Chandar et al. 2000; Rosakis et al. 2000; Geubelle and Kubair 2001; Samudrala et al. 2002; Cox et al. 2005]. Usually, experiments on how cracks start and grow are conducted with apparatus such as the Hopkinson bar; however, it produces relatively low loading rates from  $10^1$  to  $10^6 \text{ MPa m}^{1/2}\text{s}^{-1}$ . Hence, these experiments do not clearly reveal the transients of crack initiation.

Recently, Ravichandran and Clifton [1989] and Prakash and Clifton [1992] developed a plate impact technique with a high loading rate for understanding the essential fracture dynamics. This technique can produce a plane strain mode I crack using a square tensile pulse lasting less than a microsecond. It raises the loading rates by two orders of magnitude over the Hopkinson bar technique and is a noteworthy advance for the study of the transient mechanisms of material failure. However, for investigating the

---

*Keywords:* plate impact tests, dynamic fracture, failure mode transition, intersonic crack extension, discontinuous crack growth model.

The authors gratefully acknowledge the support of the National Science Foundation of China (grant nos. 10275085 and 10672166).

fracture mechanisms of mode II cracks, the technique needs to be improved. We address some aspects of this problem.

So far, restrictions in current testing technology have prevented complete understanding of the failure mechanisms in mode II fractures, notwithstanding a great number of investigations and the observation of many interesting phenomena [Kalthoff 1987; 1988; 1990; Ravi-Chandar 1995; Ravi-Chandar et al. 2000]. Kalthoff [1987; 1988] has studied the failure of high strength steel loading including dynamic mode II cracks and have shown that low speed impact induces cleavage fracture. The cracks extend at an angle of about  $70^\circ$  with respect to the original crack line, which shows that the maximum hoop stress criterion [Erdogan and Sih 1963] governs the crack initiation and growth. When the impact speed exceeds a critical value, the failure mode changes from crack fracture to shear band failure, and microscope images of the fracture surface revealed that the failure mechanism had also changed from cleavage fracture to ductile shear failure.

In similar investigations, Ravi-Chandar [1995] and Ravi-Chandar et al. [2000] demonstrated that at low loading rates, the crack tip formed a plastic zone around it, but no crack started; at moderate loading rates, a brittle crack began and the failure mode changed from ductile to brittle; and at high loading rates, the crack formed and advanced along the original crack line but was arrested in the specimen. Postmortem microstructural examination of the failure surface indicated that the maximum shear stress criterion governed the fracture process.

Elsewhere, Zhou et al. [1996] studied the initiation and propagation of shear bands by applying asymmetric mode II crack impact loading to a prenotched plate specimen. Results show that, when the impact velocity exceeds a critical value, a shear band advances throughout the specimen. When the impact velocity falls below this critical value, a shear band arrests first inside the specimen, and then a crack starts from the arrested shear band tip and grows along the propagating shear band. Under a microscope, the fracture surfaces show that a ductile mode shear failure occurs inside the shear band, and the crack fails in an opening mode. The coexistence of shear band failure and crack fracture implies that the mode II crack loading changes the failure mode from shear band failure to crack fracture.

Recently, much attention focuses on shear-dominated intersonic crack extension mechanisms. Inter-sonic cracking has been directly observed in asymmetrical impact tests on a specimen consisting of a homogeneous and isotropic solid with an artificial weak band plane [Rosakis et al. 1999, 2000], in which the shear cracks propagated initially with a speed just above the shear wave speed  $c_s$ , accelerated sharply to the longitudinal wave speed  $c_l$ , and finally approached a steady intersonic speed  $\sqrt{2}c_s$ .

Motivated by the experimental observations, many researchers have paid great attention to intersonic cracking [Needleman 1999; Abraham and Gao 2000; Geubelle and Kubair 2001; Samudrala et al. 2002]. The studies, based on continuum elastodynamics and molecular dynamics [Abraham and Gao 2000], show that when a shear crack propagates along a weak plane, a daughter crack first initiates in front of the crack tip, and then joins with the mother crack, and, as a result, the crack propagates with intersonic speeds. This conclusion has been confirmed by the fact that when a daughter crack growing at intersonic speed nucleates just ahead of the mother crack tip, the Mach cone angles at the daughter crack tip show that its velocity is consistent with the longitudinal wave speed.

The simulation study also shows that a finite peak stress ahead of the mother crack is the only possible mechanism of daughter crack nucleation. Therefore, the interaction of the “mother-daughter” crack causes a subsonic shear crack to jump over the forbidden velocity zone between the Rayleigh wave

speed  $c_R$  and shear wave speed  $c_s$ . Identical results followed from numerical calculations [Needleman 1999].

Samudrala et al. [2002] found analytical results for the subsonic and intersonic mode II crack propagation with a rate-dependent cohesive zone, indicating that the subsonic regime is inherently unstable for mode II crack propagation, but, with increasing rate sensitivity, stable mode II crack growth prevails at low subsonic speeds. At intersonic speeds, the mode II crack growth is unstable up to a critical speed higher than  $\sqrt{2}c_s$ , above which it becomes stable.

Samudrala et al. [2002] also investigated the effect on crack propagation of a dimensionless rate parameter and of shear strength of the crack plane. In the cohesive zone model, they found that fracture energy is finite at intersonic crack speeds and that more energy is dissipated when intersonic speeds are close to  $c_1$ . Furthermore, the fracture energy is sensitive to a rate parameter describing the influence of shear stress on the local sliding rate in the cohesive zone. By decreasing the crack plane strength, they found that an intersonic mode II crack would accelerate all the way up to  $c_1$ , whereas increasing it seems to favor steady crack growth with an intersonic speed close to  $\sqrt{2}c_s$ . These results agree with the crack speed characteristics observed in the experiments of Rosakis et al. [1999; 2000].

Numerical calculations by Geubelle and Kubair [2001] show an extension speed transition of a shear dominated crack from subsonic to intersonic. Usually, a rapid acceleration of the primary cohesive zone at the crack tip induces the transition. Occasionally, a secondary failure zone or perhaps a microcrack generated ahead of the crack, which quickly coalesces with the primary failure zone, can induce the transition as well. The calculations reveal that intersonic crack propagation is possible for a wide range of loading conditions, as long as the shear-dominated loading intensity is a major fraction of the strength of the fracture plane. Moreover, under mixed-mode loading conditions when the shear component of the external loading is sufficiently large, cracks can propagate intersonically. When the crack grows steadily at an intersonic speed, cohesive failure is mainly induced by shear stresses, even though the remote loading is of mixed mode.

To understand the mechanisms of mode II crack growth under high-speed impact loading, we have developed an improved plate impact testing technique and conducted dynamic failure tests of Hard-C 60<sup>#</sup> steel. The technique can generate a compressive stress pulse lasting less than a microsecond with a loading rate as high as  $10^8$  MPa  $m^{1/2}s^{-1}$ . During an asymmetrical impact, an edge crack plate specimen develops a plane strain deformation state at the crack tip. Experimental results demonstrate that the nucleation and growth of microcracks ahead of a main crack result in unstable crack propagation with nonuniform extension speeds increasing from subsonic to intersonic.

In addition, failure mode transitions, both from mode I to mode II crack and from brittle to ductile failure, were observed during the crack growth. Based on these observations, we propose a discontinuous transient crack growth model. We discuss the relevant dynamic mechanisms of crack initiation and growth, using the energy principle of dynamic fracture mechanics.

The article is organized as follows. In Section 2, we give the relevant theory for describing the crack dynamics in an asymmetrical plate. Then, in Sections 3 and 5, we describe the experimental details, including material properties, specimen configurations, the experimental setup, and the testing approach. In Section 5, we analyze under a microscope the crack growth mechanisms. Finally, we propose a discontinuous transient crack growth model for describing of intersonic crack growth qualitatively and discuss the results.

## 2. Theoretical background

The dynamic fracture process displays many complex features, such as the response of material crystal and atomic structures, inelastic properties, microdefects, strain rate sensitivities, and so on; however, moving crack tips in a variety of materials all exhibit the phenomena of crack initiation, kinking, and bifurcation, all of which are assumed to occur in continuous media. Thus, we can still effectively use continuum mechanics for describing the essential dynamic failure mechanisms. Here, we present the elastic wave theory [Achenbach 1973] as the theoretical basis for improving the plate impacting technique. Then, we use the energy methods of elastodynamic fracture theory [Freund 1990] and the analytic results of the linear elastodynamic problem [Ma 1998] to interpret the failure mechanisms of materials and investigate the behaviors of crack growth.

With the asymmetrical plate impact technique, it is easy to produce a mode II crack deformation field in an edge crack plate specimen. Such a specimen is effectively simulated as semiinfinite crack tip field in an infinite elastic body. It is reasonable to assume that one-dimensional stress waves propagate during the collision. Furthermore, we assume that no incident stress pulses reflect from the component interfaces because all collision components have the same impedance and they are joined without gaps. Figure 1 illustrates a distance-time ( $x, t$ ) diagram of the stress wave fronts prevailing in the collision and the smaller velocity-stress ( $v, \sigma$ ) diagram characterizing each region in the ( $x, t$ ) diagram. The figure shows that at time  $t_3$  two unloading stress pulses meet in the momentum trap, and create a tension stress pulse. At time  $t_4$ , when the pulse reaches the interface between the specimen and the momentum trap, the interface splits and the momentum trap separates from the specimen. Because the momentum trap is thicker than the flyer, it can trap the entire tensile pulse. Thus, the flyer transfers its momentum to the momentum trap, and, in the collision process, the specimen feels only the impact of a single duration compressive stress pulse. In addition, the diameter-to-thickness ratio of the specimens is chosen larger

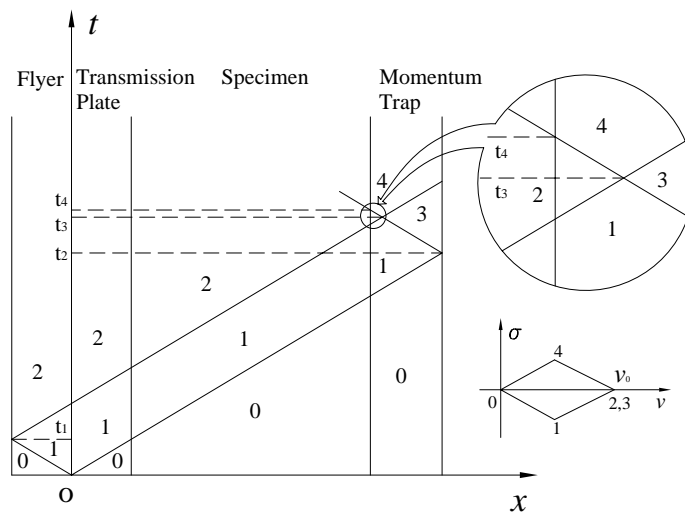


**Figure 1.** Distance-time ( $x, t$ ) diagram in the asymmetrical plate impact procedure, with velocity-stress ( $v, \sigma$ ) illustrated in the inset.

than four, effectively reducing the effect of their boundaries on crack growth. These measures ensure that a plane strain mode II crack deformation field develops in the central region of the edge crack plate specimen, which can be confirmed in the microscope images of the fracture surface described below.

In asymmetrical impact loading, strictly speaking, a transient mixed-mode deformation field develops at the crack tip, in which the mode II crack deformation field predominates because of the shear effects produced by the high strength compressive stress pulses; however, a time-dependent mode I deformation weak field also forms [Freund 1990]. Figure 2 illustrates the wavefront for the stress pulse scattered by the crack tip when the impact is shorter than  $2l/c_1$ . Generally, a longitudinal plane pulse (1) induces a mode II crack deformation field; the competition between the inertial resistance and Poisson's effect creates a mode I deformation weak field, and the cylindrical waves (2)–(8) generate a mixed-mode deformation field. In this study, we directly measure variations of the compressive stress pulses using the Mn-Cu gauge technique [Raiser et al. 1990; Fowles et al. 1970]. To validate the measurements, we compare the amplitudes of stress pulses with the calculated values based on the measured impact speeds  $V_0$  and the elastodynamic relation,  $\sigma_0 = \rho c_1 V_0/2$ .

The energetics relevant to dynamic fracture are briefly described below; more details can be found in [Freund 1990]. For mixed-mode crack growth at nonuniform speed  $v$ , the dynamic energy release rate is given by

$$G = \frac{1 - \mu^2}{E} [A_I(v)K_I^2 + A_{II}(v)K_{II}^2], \tag{2-1}$$

where

$$A_I(v) = \frac{v^2 \alpha_d}{(1 - \mu)c_s^2 D}, \quad A_{II}(v) = \frac{v^2 \alpha_s}{(1 - \mu)c_s^2 D},$$

$$D = 4\alpha_d \alpha_s - (1 + \alpha_s^2)^2, \quad \alpha_d^2 = 1 - v^2/c_l^2, \quad \alpha_s^2 = 1 - v^2/c_s^2.$$

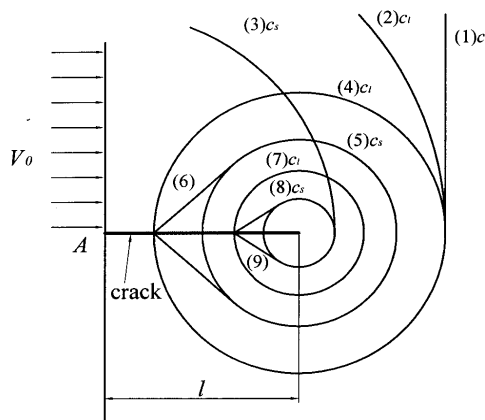


**Figure 2.** The wave fronts of the stress pulses scattering by the crack tip in the asymmetrical impact procedure.

The dimensionless functions  $A_I(v)$  and  $A_{II}(v)$  are universal functions of the crack speed  $v$  and the properties of the materials. They do not depend on the load or the crack body configuration.  $E$  and  $\mu$  are the Young's modulus and Poisson's ratio.  $K_I$  and  $K_{II}$  are the time-dependent stress intensity factors of mode I and II with the instantaneous crack length  $vt$ . According to Griffith's critical energy release rate criterion, a crack must extend so that the crack tip releases energy at a rate equal to the dynamic fracture energy of the material. Hence, under isothermal conditions, the growth criterion is  $G = \Gamma$ , where  $G$  is the energy release rate and  $\Gamma$  is the special fracture energy of arbitrary crack growth at nonuniform speed. (These standard descriptions of  $G$  and  $\Gamma$  are more intuitive than precise, as they have dimensions of energy per area or force per length.) Generally,  $G$  is a property of the local mechanical field of the crack tip; it represents the effect of applied loading, the body configuration, and bulk material parameters.  $\Gamma$  characterizes resistance to crack extension and is related to the current crack length and speed.

A theoretical study by [Lee and Freund \[1990\]](#) analyzed the two-dimensional elastodynamic problem of a semiinfinite plate containing a static edge crack under asymmetrical impact loading with a normal velocity imposed suddenly on one side of the edge cracked plate. By using a universal function of the crack growth speed and the static stress intensity factor, the time-dependent stress intensity factors  $K_I$  and  $K_{II}$  are expressed as

$$K_I(t, l, v) = k_I(v)K_c(t, l, 0), \quad K_{II}(t, l, v) = k_{II}(v)K_c(t, l, 0)$$

in which  $K_c(t, l, 0) = \lambda/(2\pi l)^{1/2}$ ,  $k_I(v)$  and  $k_{II}(v)$  can be found in [[Lee and Freund 1990](#); [Ravi-Chandar et al. 2000](#)], and  $\lambda$  is proportional to the stress pulse amplitude. Here, it is assumed that the results can generalize for the situation of dynamic crack growth. That is, the stress intensity factor is a function of crack length and time, as well as the crack speeds. Thus, we use the time-dependent intensity factors  $K_I$  and  $K_{II}$  of [Equation \(2–1\)](#) to evaluate the crack growth speeds and dynamic stress intensity factors.

### 3. Experimental details

**3.1. Materials.** We test Hard-C 60<sup>#</sup> steel. Because its behavior reveals clear rate-dependent characteristics in dynamic loading, it is a suitable material for examining how loading rates affect macroscopic and microscopic failure. The material properties of Hard-C 60<sup>#</sup> steel are given in reference [[Ma and Duan 2000](#)]. Before testing, the material was normalized at 880° C, quenched rapidly in oil, and then tempered at 200° C for 3 hours. The treatment created a relatively homogeneous martensitic microstructure, significantly increasing the yield limit. Uniaxial tensile tests, under loading at a strain rate of  $10^{-1} \text{ s}^{-1}$ , show that the yield stress increases from 420 MPa to about 580 MPa. Quasistatic three-point bending tests show that the fracture toughness is about 55.2 MPa m<sup>1/2</sup>. [Figure 3](#) shows a SEM image of the quasistatic fracture surface. It clearly reveals cleavage fracture traits. Measurements indicate that the average hardness has reached 54 HRC, which is brittle enough for our purposes. Hence, we can assume that the plastic deformation region, if it even exists at the dynamic crack tip, is negligibly small, and that the results of impacting experiments can be interpreted using elastodynamic fracture theory outlined in the previous section.

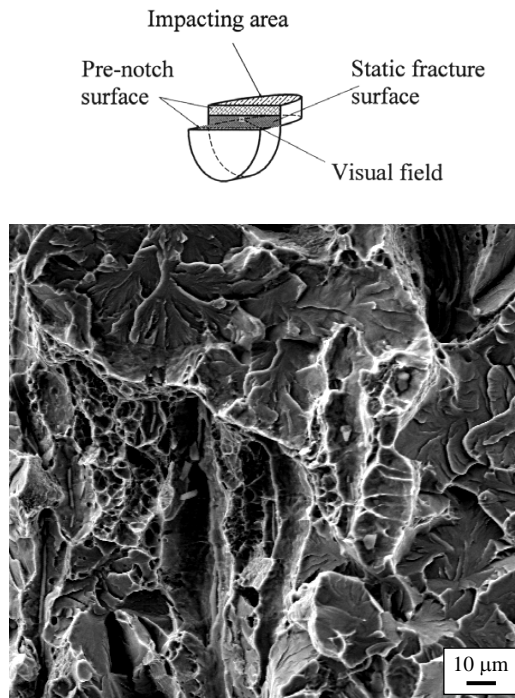


**Figure 3.** The SEM picture of the brittle fracture surface of the opening mode cracks under the quasistatic three-point bending loading conditions. The inset shows the corresponding visual field.

#### 4. Components in the collision system

To create a plane strain state at the crack tip in the edge crack plate specimen, we employ a special impact system consisting of the flyer, specimen, transmission plate, and momentum trap. The geometry of the impact components is shown in Figure 4. The single edge-notched specimen is a round disc 50 mm in diameter and 10 mm thick. The initial notch about 5 mm long and  $150\ \mu\text{m}$  wide is cut by electric discharge machining; see Figure 4a. The other components are half round discs with same material and radius, but with different thickness (see again Figure 4). Before the impact tests, all component surfaces were machine-lapped flat using 3–15  $\mu\text{m}$  diamond powder papers and then polished on Texmeth cloth over a flat plate using a 0.1–0.3  $\mu\text{m}$  diamond paste. The process ensured the surfaces were flattened to an accuracy better than one Newton's ring.

**4.1. Experimental setup.** The experiment consists of the following: a pressure-shear gas gun for producing the compressive stress pulses; Mn-Cu stress gauge units for directly measuring the compressive stress-time profiles [Ma 1998]; a soft recovery apparatus [Raiser et al. 1990]; two electrical circuits, one for measuring the projectile impact velocities and another for examining the misalignment angles between the impacting planes.

The pressure-shear gas gun has a launch tube 60 mm in diameter and 6 m long. A keyway runs along the tube's length to prevent the projectile from rotating during firing. The main part of the projectile is a

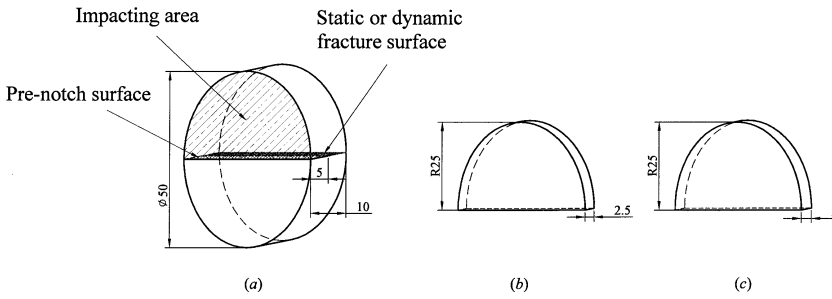


**Figure 4.** The configurations and geometries of the crashing components used in this study, including the specimen (a), transmission plate and flyer (b), and momentum plate (c).

high-density plastic foam column 58 mm in diameter and 0.25 m long. Its front face is bonded to the flyer and its rear end is connected an aluminum tail that holds two sealing O-rings and a key fit to the keyway. Because the plastic foam has much lower impedance than the flyer, it can be taken for granted that the compressive stress pulse is reflected into the tensile unloading pulse at the bond interface between the flyer and the plastic projectile.

Figure 5 shows the experimental configuration schematically. The target assembly consists of an inner ring supporting the specimens and an outer tapped ring connected to a holder. The holder system is designed so that it can be accurately adjusted with small translations along the three axial directions and small rotations in the three angle coordinates. (See the inset in Figure 5). Thus, the relative position and orientation of the flyer and the specimen can be precisely fixed before the impact tests. A heavy steel anvil is placed ahead of the momentum trap to reduce the influence of the projectile's impulse. During impact, the projectile momentum consists of two parts: one from the fast moving flyer and another from its aluminum tail. In first collision stage, that is, when the flyer hits the transmission plate, the flyer imparts its momentum to the momentum trap, causing stress wave propagation, but is then taken away after it separates from the specimen. In this way, we prevent the tensile unloading pulse from again loading the specimen and ensure that it is only loaded with a single pulse. In the later stage of impact,

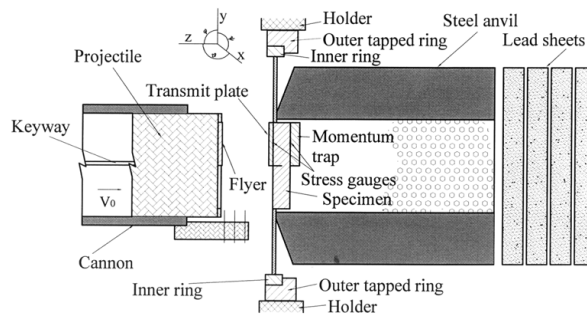


**Figure 5.** The schematic of the target assembly.

the aluminum tail hits the steel anvil and transfers its momentum to the steel anvil. Energy is further dissipated through the plastic deformation of lead sheets located in the other end of pressure chamber; see [Figure 5](#). The steel anvil then contains specimens which can be easily seen and recovered intact for the postmortem microscopic analysis.

**4.2. Experimental procedure.** The impact test takes place in a pressure chamber which can sustain a gas pressure up to 16 MPa. Prior to the test, it is evacuated to a pressure of  $2\text{--}3 \times 10^{-6}$  Pa, and, during the test, its internal pressure remains at  $2\text{--}5 \times 10^{-5}$  Pa. The inclination pitch between the flyer's impacting planes and the target plate is measured using a tilt system consisting of three pairs of pins and an amplifying circuit. The measurements show that the inclination pitches are well controlled on the order of  $2\text{--}4 \times 10^{-5}$  radians. The impinging velocities of the flyer are initialized by the method described in [\[Fowles et al. 1970\]](#); the largest measured relative difference among the impact velocities is less than 2 percent. The Mn-Cu stress gauge technique [\[Ma 1998\]](#) is used to measure how the compressive stress varies with time at impact. Gauges are embedded at two interfaces of the collision system; one is in front of the specimen and another is behind it (see [Figure 5](#)). For each shot, a TPM3323 oscilloscope records two sets of compressive stress-time data. We use the data for analyzing the experimental results in the following section.

## 5. Experimental results and discussion

In the impact experiment, we conducted nine shots with the asymmetrical plate impact technique. We observed two different types of failure mechanisms when the impact velocity increased from 150 m/s to 210 m/s. At velocities less than 180 m/s, only crack fracture occurs. As the impact velocity is increased into the range of 190–210 m/s, a complex failure takes place involving both crack fracture and microcavity damage in the crack tip field. The former catches our attention in this article, but we may consider the latter in the future. This result shows that the failure behaviors are closely related to the loading rates.

[Figure 6](#) shows the compressive stress-time profiles of two shots at the impact velocities of 173 m/s and 204 m/s. It is clear that the stress pulses last for less than a microsecond and approach very nearly the theoretical value 830 ns. The pulse rise time is less than 200 ns. In this figure, the curve with the higher peak stress is the input stress pulse measured at the interface between the transmission plate and the specimen, and the curve with lower peak stress is the output stress pulse measured at the interface between the specimen and the momentum trap. The dissimilarity between the two stress pulse profiles *a* and *b* (see [Figure 6](#)) implies that more mechanical energy flows into the specimen than out of it. Therefore, some mechanical energy is dissipated as the internal structure changes through microcrack formation, crack growth, plastic flow and microcavity damage. Note from the figure that a larger difference of the amplitudes of stress pulses usually presents before the peak compressive stress is reached. This indicates that dissipation of mechanical energy and change of material microstructure has already taken place during the first half of the stress pulses. At low impact speed (see [Figure 6a](#)), the similarity between the curves suggests that the stress pulses induce an elastodynamic response and only uncomplicated failure mechanisms such as crack growth occur; at high impact speed (see [Figure 6b](#)), the differing curves indicate that more complex failure mechanisms occur, involving not only crack growth, but also plastic softening and material damage. [Ma and Duan \[2000\]](#) report related results in detail.

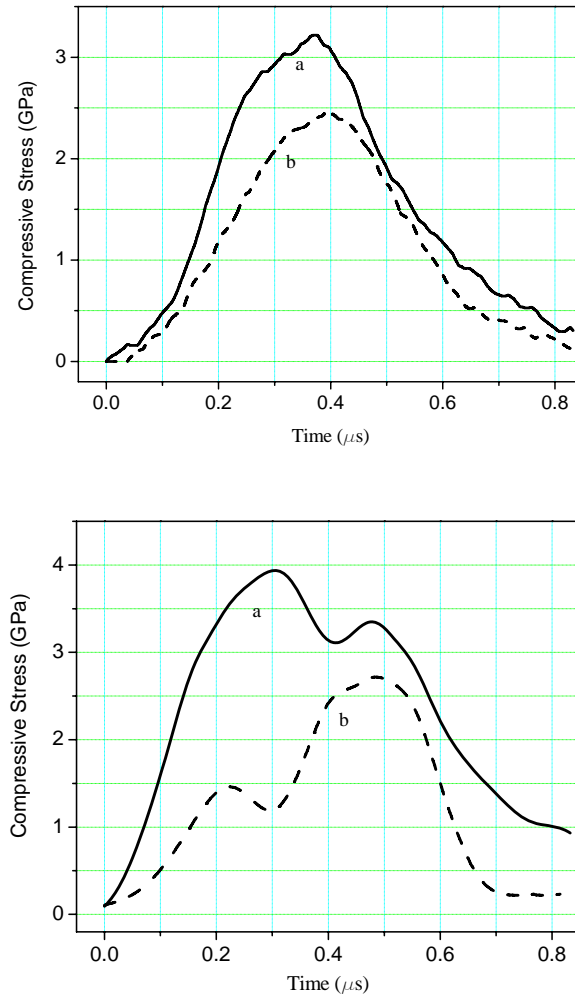


**Figure 6.** The compressive stress-time functions measured by Mn-Cu stress gauges, at impact velocities of 173 m/s (the first figure) and 204 m/s. The curve *a* represents the gauges embedded at the interface between the transmission plate and specimen, and the curve *b* is for gauges between the specimen and momentum plate.

Figure 7 shows the SEM images of the fracture surface when the impact speed was 173 m/s. The fracture surface consists of three distinct regions: a prenotched region, a dynamic fracture region, and a static fracture region. The uniform dynamic crack growth region suggests that a plane strain state at the extending crack tip prevails during impact. Figure 8 shows the corresponding SEM picture of the crack growth path, which has a straightforward interpretation as a discontinuous extension mechanism of moving cracks. Clearly, the crack grows in two stages. During the first, the crack begins to form at the notch tip on the impacting side and extends about  $130 \mu\text{m}$  normal to the notch periphery before kinking. Because the loading rate is high enough, the stress intensity factor of the notch tip field reaches the material's fracture toughness and initiates a crack. Additionally, because the notch tip lacks surface

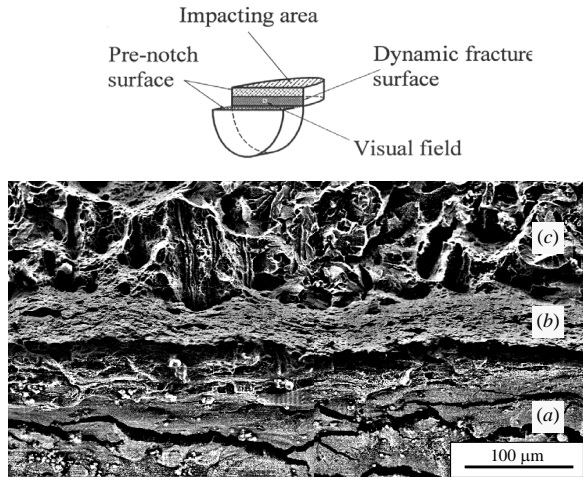


**Figure 7.** The SEM picture taken from the central region of the specimen fracture surface. The inset shows explicitly the fracture mechanism of the plane strain state at the crack tip.

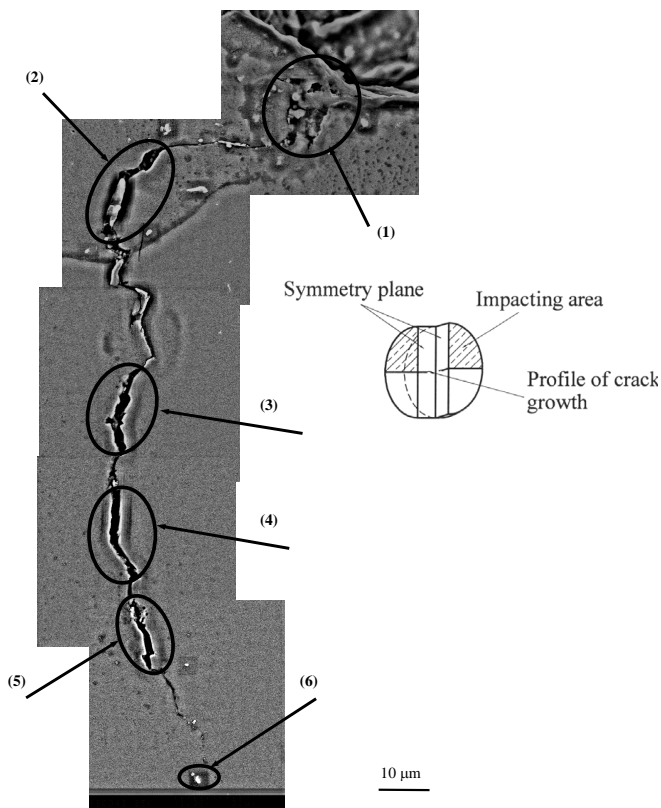


**Figure 8.** As seen under a microscope, the main crack interacting with the microcracks. The visual field is located in the sample's symmetry plane.

traction, the crack must be initiated by the hoop tensile stress, whose the intensity has gone beyond the yield limit, resulting in plastic softening. It seems clear that the cracks have started through the ductile initiation mechanism. This conclusion is also supported strongly by the residual opening displacement of the crack face indicated by the ellipse (1) in the figure. Moreover, in our prior impact experiments [Ma and Duan 2000], we have observed that the angle of crack initiation relative to the original prenotch line is approximately  $55^\circ$ , which does not deviate far from the location of crack initiation observed in [Ravi-Chandar 1995; Ravi-Chandar et al. 2000], nor from the point of maximum circumferential stress calculated by [Lee and Freund 1990]. Evidently, the geometry the notch tip and the mechanism of the plastic softening are responsible for the slight discrepancy. Furthermore, the crack extends approximately normally to the notch periphery. This suggests that the crack growth mechanism is dominated by mode I cracking at this time even though the intense compressive stress pulse generates a mixed-mode stress field at the crack tip. The first image in Figure 9 magnifies the fracture surface. Comparing the observed features with the static brittle features shown in Figure 3, we see that the crack growth behaviors exhibit obvious cleavage characteristics. Therefore, in this stage, the mode I crack begins and grows by different mechanisms, that is, by ductile initiation and brittle growth. The maximum hoop stress criterion [Ravichandran and Clifton 1989] causes these to mechanisms occur.

In the second stage, the growing crack changes its extension orientation from perpendicular to the notch periphery to compressive stress pulse propagation. That is, the crack grows along the original crack line on which shear stress is maximal. Hence, the maximum shear stress criterion now governs the

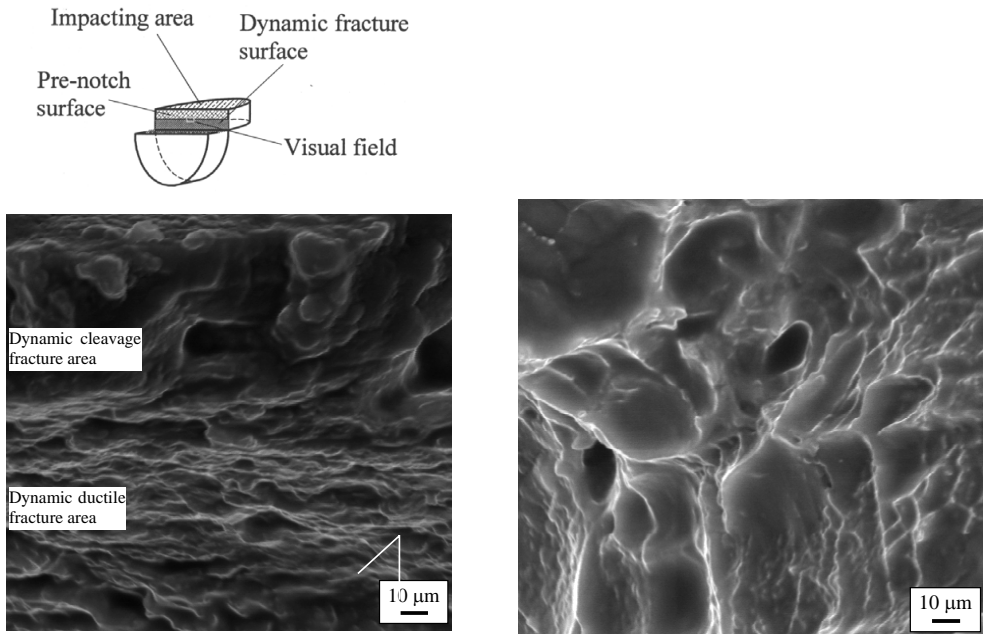


**Figure 9.** Microscopic image of the dynamic fracture surface after mode I cracking illustrates ductile cracking under asymmetrical impact conditions; the view field is above. The second image illustrates the same, but with mode II cracking.

crack extension. Microscopic images of the dynamic fracture surface (see the second image in [Figure 9](#)) show extensive dimpling and drawing, implying that ductile fracture has become the dominant failure mechanism. Actually, it is the large shear stress on the crack line that induces the heating and plastic softening. From the discussion above, we conclude that the crack fracture extension mode has undergone a transition from mode I to mode II, and the failure mode has also experienced a complex change from ductile initiation, to brittle growth, and back again to ductile growth, after the dominant stress driving the crack growth changes from the maximum hoop tensile stress at the crack tip to maximum shear stress along the crack line.

From the experimental results obtained above, we have seen that two crucial mechanisms of the crack growth need further attention. The first is the kinking phenomenon along a curved path. It should be noted from [Figure 8](#) that the crack kinking occurs at the point where the mode I crack growth ends and the mode II crack growth starts, as indicated by the ellipse marked (2). On the one hand, the asymmetrical impact loading produces an elastic, perhaps following plastic, compressive stress pulse that propagates as a plane pulse in the impacted side of the specimen. When the pulse reaches the notch tip, an unloading tensile pulse is generated due to the dispersion the stress wave. Because the impact speed is high, the consequent tensile pulse is strong enough to induce mode I crack initiation and growth. As the energy dissipation needed for crack growth increases, the intensity of the hoop tensile stress decreases rapidly; in contrast, the shear stress intensity increases quickly. As the hoop stress becomes weaker than the shear stress, shear stress effects begin to dominate the crack growth. On the other hand, inherent flaws in the material, such as those marked by ellipse (2) [Figure 8](#), can also potentially cause the crack to kink. At very least, these flaws favor crack kinking. Evidently, both the local mechanical field and the internal structure of the material can cause crack kinking.

The second crack growth mechanism is one of discontinuous extension. During the impact process, the precursor of the compressive stress pulse first makes the material flaws nucleate, grow, and develop into a number of microcracks. Then, the shear stress acting along crack line initiates and extends microcracks ahead of main crack. Finally, these microcracks develop into a series of macroscopic subcracks. Subsequently, the interaction and coalescence of these subcracks result in an unsteady advance of the main crack. This extension mechanism can be clearly seen from the crack growth path illustrated in [Figure 8](#). Material flaws are marked by six ellipses numbered (1)–(6). These nuclei develop later into microcracks. At the bottom, mark (6) denotes a microcavity, near which the crack has arrested but not yet coalesced. This demonstrates that several mechanisms are active as the unsteady crack extends. For instance, when the main crack interacts with mature microcracks near the crack tip and coalesces with them, the remaining microcracks a bit farther from the crack tip simultaneously nucleate and grow due to the shear stress, and then the subsequent interaction and coalescence of the cracks result in the discontinuous crack growth. In the present example, the high intensity stress pulses have caused five subcracks to nucleate and grow, exhibiting the entire process of unsteady crack extension. In the low speed shots of our experimental study [[Ma and Duan 2000](#)] and other previous studies [[Ravi-Chandar and Knauss 1984](#)], authors observed and investigated theoretically [[Abraham and Gao 2000](#); [Needleman 1999](#)] only the interaction between the main crack and one subcrack ahead of the crack tip. However, it is worthwhile to investigate the mechanisms of multiple subcrack nucleation and growth. We hope that more interesting mechanisms of crack growth will be revealed which would probably not be found when only studying the interaction between a main crack and a single subcrack.

### 6. Discontinuous transient crack growth model

During an asymmetrical impact of an edge crack plate specimen, the flyer’s kinetic energy is transformed into the total impact energy of the collision system in such a way that compressive stress pulses enter the specimen at the face hit by the flyer and exit from other face into the momentum trap (see Figure 5). This implies that both positive and negative work have been done on the specimen body during the impact. Precisely, the former is equal to the kinetic energy of flyer and the latter is the kinetic energy of the momentum trap. Clearly, the net work adds to the internal energy of the material and dissipates through mechanisms such as crack growth, plastic deformation, and material damage. The energy equilibrium condition for the process [Freund 1990] is

$$\int_{t_1}^{t_2} \int_{S_1} \sigma_{ij}^{(1)} n_j^{(1)} \frac{\partial u_i^{(1)}}{\partial \tau} dS_1 d\tau - \int_{t_1}^{t_2} \int_{S_2} \sigma_{ij}^{(2)} n_j^{(2)} \frac{\partial u_i^{(2)}}{\partial \tau} dS_2 d\tau = \int_{t_1}^{t_2} F_C d\tau, \tag{6-1}$$

where  $S_i$  ( $i = 1, 2$ ) are the plane curves around the areas affected by the compressive stress pulses  $\sigma^{(i)}$ .  $\Delta t = t_2 - t_1$  is the pulse time interval. The two terms on the left side of the equal sign in Equation (6-1) represent the positive and negative work done by the stress pulse in the interval, and therefore, the right side becomes the net work and is equal to the total energy dissipated in the specimen as the material responds to the dynamic loading. If we are only considering the crack growth mechanism and neglecting other energy dissipation mechanisms such as plastic deformation and material heating, the integrated function  $F_C$  is the instantaneous rate of energy flow toward the crack tip contour  $C$  through a small contour around it. The energy dissipation rates can be determined from the energy equilibrium relation Equation (6-1) and the compressive stress-time curves (see Figure 6). They are shown in Figure 10. The figure shows that the energy dissipates in four stages. The first corresponds to rapid energy dissipation (O–A in Figure 10), which suggests that not only the first subcrack initiates and grows but that other subcracks, such as the second and third, also initiate and advance, one after the other. Hence,

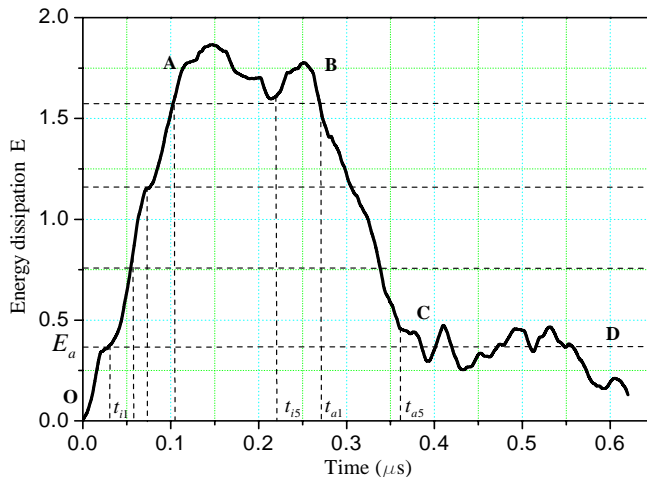


**Figure 10.** The energy dissipation rates are obtained from the measured stress pulse time series.

a great quantity of energy dissipates through the crack forces. In the second stage (A–B in Figure 10), the energy dissipation becomes much more stable, implying either that no new subcracks form or that some do but arrest immediately. In the third stage (B–C in Figure 10), an abrupt decrease in energy dissipation implies that the subcracks have coalesced and the main crack has stalled in the specimen. In the last stage (C–D in Figure 10), energy dissipates at a constant low level, suggesting the process of crack growth has stopped. The energy put into crack initiation and growth is mainly associated with the first three stages of the energy dissipation process.

The main, rapidly propagating crack consists of five subcracks with lengths  $l_k$  ( $k = 1, 2, \dots, 5$ ) (see Table 1). For simplicity, we assume that the subcracks grow at constant velocity after they form and dissipate energy each in proportion to its length. Thus, each subcrack grows steadily, but the main crack advances unsteadily with nonuniform velocities due to the different initial time and growth rate of each subcrack. Each subcrack dissipates energy  $G_k$ :

$$G_k = C_k \int_{t_k^i}^{t_k^a} [E(t) - E_a] dt, \quad C_k = l_k/l, \tag{6-2}$$

where  $E(t)$  is the current rate of energy dissipation of crack growth.  $E_a$  and  $l$  are the rate of energy dissipation of the crack arrest and the length of the main crack. If the critical energy release rates for crack initiation are assumed to be equal to those of the crack arrest fracture energy, then the initiation times  $t_k^i$  ( $k = 1, 2, \dots, 4$ ) of the first four subcracks can be determined from the energy dissipation in Figure 10, and the corresponding ending times of subcrack growth,  $t_k^a$  ( $k = 1, 2, \dots, 4$ ), can be determined by integrating the equations for dynamic crack tip motion Equation (2-1) and using the relation (6-2) as

$$\frac{1 - \mu^2}{E} \int_{t_k^i}^{t_k^a} [A_I(v)K_I^2 + A_{II}(v)K_{II}^2]v dt = \Gamma_k, \tag{6-3}$$

Experimental results in this study		Results based on the dynamic fracture theory <sup>†</sup>			Results obtained from the elastodynamic problem <sup>††</sup>		
No. ( $k$ )	$l_k$ (mm)	$V_k^a$ (mm/ $\mu$ s)	$t_k^i$ (ns)	$\Delta t_k$ (ns)	$V_k^a$ (mm/ $\mu$ s)	$t_k^i$ (ns)	$\Delta t$ (ns)
1	0.132	1.34	168	98.51	1.59	168	83.02
2	0.128	1.47	198	87.10	1.77	198	72.32
3	0.048	2.82	220	17.02	2.49	220	18.28
4	0.068	2.73	245	24.91	2.21	245	30.77
5	0.076	2.54	352	29.92	1.97	337	38.58

**Table 1.** Characteristic parameters of each subcrack. Here the  $l_k$  ( $k = 1, 2, \dots, 5$ ) are the lengths of five subcracks.  $t_k^i$ ,  $V_k^a$ , and  $\Delta t_k$  are the initial time, average velocities, and interval of time for growth of each subcrack. <sup>†</sup>[Freund 1990]; <sup>††</sup>[Lee and Freund 1990].

for  $k = 1, 2, \dots, 5$ , where  $\Gamma_k = G_k/l_k$  is the mechanical energy flowing into the subcrack tip per unit crack advance length. For the last subcrack, the arrest time  $t_5^a$  can be determined directly from Figure 10, and its initiation time  $t_5^i$  can be obtained from (6–3). Table 1 shows the results.

Figure 11 shows the lengths of the subcracks and the positions of the main crack tip at times,  $t_k^i$ , ( $k = 1, 2, \dots, 5$ ). The first shows results of the dynamic fracture theory [Freund 1990], and the second shows analytic results of the idealized elastodynamic problem [Lee and Freund 1990]. As the first subcrack is advancing (with an average velocity of  $V_1^a$ ), the compressive stress pulses propagating at the longitudinal wave speed 6020 m/s arrive at the initial location of the second subcrack, causing it to initiate at time  $t_2^i$ . This implies that, on the macroscopic scale, the main crack grows suddenly longer and

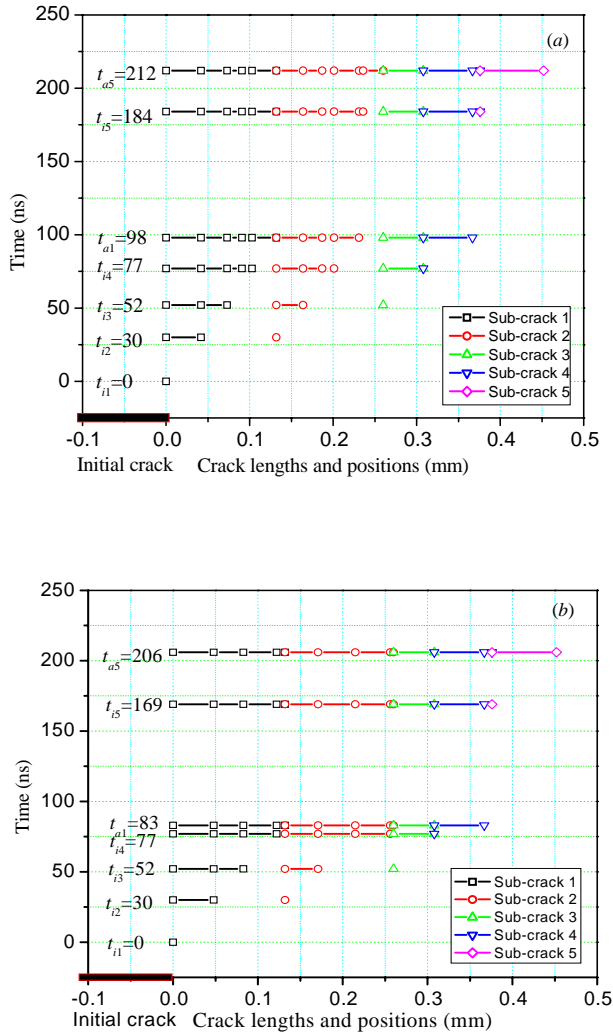


**Figure 11.** The lengths of the subcracks and the site of the main crack tip at characteristic times. (a) displays the analytic results from classical dynamic fracture theory and (b) is that of Lee and Freund [1990].

the growth velocities jump discontinuously from slow to fast. Note that, at this time, the second subcrack tip replaces the first subcrack tip to become the main crack tip. In the same way, subsequent initiation and growth of other subcracks induce crack growth velocity jumps. By assuming that the behavior of each subcrack follows from the elastodynamic theory of continuum mechanics, we explain the unsteady growth of the main crack by some interesting features in the history of the extension velocities.

By fitting results in Figure 11 to curves, we can obtain crack tip positions as a function of time. By differentiating, we find speed versus time, illustrated in Figure 12. At  $t_1^i$ , crack growth begins. Only the first subcrack has started. Its uniform speed  $V_1^a$  completely determines the overall growth rate and the initiation of the main crack. Then, as other subcracks begin to form and grow, the main crack grows faster and more erratically: its speed goes from constant subsonic speeds less than Rayleigh wave speed  $c_R$  to nonuniform intersonic speeds higher than shear wave speed  $c_s$ . After that, some of the subcracks stop growing, but a few that extend continuously into the main crack continue to grow steadily for about 100 ns at an intersonic speed near  $\sqrt{2}c_s$ . Finally, when the first several subcracks stop advancing and coalesce, the main crack growth is completely governed by the last, unsteadily growing, subcrack. The extending speed quickly decreases to subsonic levels, and the cracking ceases.

The theoretical and numerical simulation studies [Needleman 1999; Rosakis et al. 1999; 2000; Abraham and Gao 2000; Geubelle and Kubair 2001] have shown two key characteristics of intersonic crack growth: (i) if crack growth speed is between  $c_R$  and  $c_s$ , the energy release rate of the moving crack tip is negative, and elastodynamic fracture energy theory cannot describe the mechanisms of unsteady intersonic crack growth; (ii) the steady growth speed of a mode II crack should be either subsonic (that is, lower than  $c_R$ ) or intersonic (higher than the  $c_s$ ), but stable intersonic growth speed will consistently come close to a constant speed of about  $\sqrt{2}c_s$ . Based on the discontinuous crack growth model, we can conclude that the initial compressive stress pulses control the subcrack initiation. Actually, whether the subcrack can initiate under asymmetrical impact loading depends completely on the energy flux toward the crack tip, that is, the intensity of the stress pulse. The initial time is closely related to the propagation speed of the stress pulse. Here, the compressive stress pulse propagates at the longitudinal wave speed,

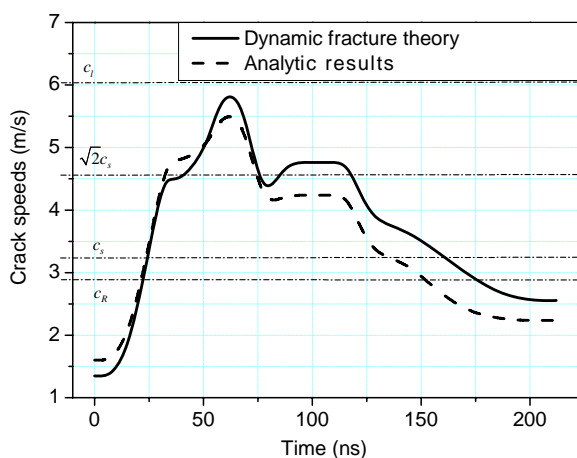


**Figure 12.** The speed-time profiles of the main crack growth from the interacting transient cracking model.

which in all probability makes the subcracks initiate continuously in short time intervals competing with the arrival of the longitudinal wave. Hence, the continuous initiation and growth mechanisms of several subcracks ahead of the crack tip lead to an extremely rapid increase of the crack growth speed, which is responsible for the transition from subsonic to intersonic.

Generally, the theory of continuum mechanics can effectively predict the growth of a single crack; however, it is too limited to explain the simultaneous initiation and growth of several cracks. This is possibly the source of the nonsensical negative energy release rate. However, using the discontinuous crack growth model put forward here, this nonsense is straightforwardly and reasonably interpreted. Moreover, we have seen that the successive growth and coalescence among the subcracks make the main crack grow steadily at intersonic speeds of about  $\sqrt{2}c_s$ , but the reason for this specific speed cannot yet be understood clearly through qualitative analysis based on the discontinuous crack growth model. Quantitative understanding of intersonic crack growth will require more delicate and profound theoretical analysis and numeral simulation. In conclusion, the discontinuous transient crack growth model can explain very well why the crack growth speed quickly increases from subsonic to intersonic and can at least qualitatively describe the various features of the intersonic crack growth.

## 7. Conclusion and remarks

We summarize as follows:

- (1) We developed a recoverable plate impact experiment with loading rate of  $10^8 \text{ MPa m}^{1/2}\text{s}^{-1}$  for studying the mechanisms of the shear dominated crack extension. Using this technique, we can generate a single compressive stress pulse of submicrosecond duration and produce a plane strain deformation field at a mode II crack tip in the edge crack plate specimen.
- (2) The dynamic fracture testing results of Hard-C 60<sup>#</sup> steel indicate that the stress pulse can induce several microcracks ahead of the crack tip to nucleate and grow simultaneously and to finally develop into macroscopic subcracks. The interaction and coalescence of these subcracks is responsible for unsteady extension of the shear dominated cracks. We inferred failure mode transitions, both from a mode I to mode II crack and from cleavage to ductile fracture.
- (3) We established a discontinuous transient crack growth model and analyzed the unstable extension of the shear dominated cracks with discontinuously varying extension speeds. The model describes qualitatively the main characteristics of the intersonic crack extension, such as the forbidden speed region between  $c_R$  and  $c_s$ , and the steady limit speed  $\sqrt{2}c_s$  when the crack growth rates increase from subsonic to intersonic. The results show that transient mechanisms such as the nucleation, interaction and coalescence among the subcracks cause the main crack extension speed to rapidly exceed the forbidden speed and that subsequent stable growth of subcracks cause the intersonic growth of the main crack.

## Acknowledgements

We extend our gratitude for many helpful discussions and guidance on English writing to Professor Keren Wang and Professor Lanhong Dai of the Institute of Mechanics in the Chinese Academy of Sciences.

## References

- [Abraham and Gao 2000] F. F. Abraham and H. Gao, “How fast can crack propagate?”, *Phys. Rev. Lett.* **84**:14 (2000), 3113–3116.
- [Achenbach 1973] J. D. Achenbach, *Wave propagation in elastic solids*, North-Holland, Amsterdam, 1973.
- [Cox et al. 2005] B. N. Cox, H. Gao, D. Gross, and D. Ritted, “Modern topics and challenges in dynamic fracture”, *J. Mech. Phys. Solids* **53**:3 (2005), 565–596.
- [Erdogan and Sih 1963] F. Erdogan and G. C. Sih, “On the crack extension in plates under plane loading and transverse shear”, *J. Basic Eng. (Trans. ASME)* **85**:4 (1963), 519–527.
- [Fowles et al. 1970] G. R. Fowles, G. E. Duvall, J. Asay, P. Bellamy, F. Feismann, D. Grady, T. Michaels, and R. Mitchell, “Gas gun for impact studies”, *Rev. Sci. Instrum.* **41**:7 (1970), 984–996.
- [Freund 1990] L. B. Freund, *Dynamic fracture mechanics*, Cambridge University Press, Cambridge, NY, 1990.
- [Geubelle and Kubair 2001] P. H. Geubelle and D. V. Kubair, “Interersonic crack propagation in homogeneous media under shear-dominated loading: numerical analysis”, *J. Mech. Phys. Solids* **49**:3 (2001), 571–587.
- [Kalthoff 1987] J. F. Kalthoff, “Shadow optical analysis of dynamic shear fracture”, pp. 16–21 in *Proc. int. conf. on photo-mechanics and speckle metrology*, San Diego, CA, Aug. 1987.
- [Kalthoff 1988] J. F. Kalthoff, “Shadow optical analysis of dynamic shear fracture”, *Opt. Eng.* **27** (1988), 835–840.
- [Kalthoff 1990] J. F. Kalthoff, “Transition in the failure behavior of dynamically shear loading cracks”, *Appl. Mech. Rev.* **43**:5 (1990), S247–S250. Part. 2.
- [Lee and Freund 1990] Y. J. Lee and L. B. Freund, “Fracture initiation due to asymmetric impact loading of an edge cracked plate”, *J. Appl. Mech. (Trans. ASME)* **57** (1990), 104–111.
- [Ma 1998] W. Ma, *Experimental and theoretical studies on the dynamic fracture toughness of materials under pressure-shear combined stress waves*, PhD thesis, Institute of Mechanics of CAS, 1998.
- [Ma and Duan 2000] W. Ma and Z. Duan, “The investigation on dynamic fracture behavior of materials under compressive-shear combined stress waves”, *Acta Mech. Sin.* **16**:4 (2000), 335–346.
- [Needleman 1999] A. Needleman, “An analysis of intersonic crack growth under shear loading”, *J. Appl. Mech. (Trans. ASME)* **66**:4 (1999), 847–857.
- [Prakash and Clifton 1992] V. Prakash and R. J. Clifton, “Experiment and analytical investigation of dynamic fracture under conditions of plane strain”, pp. 412–444 in *Fracture mechanics: twenty-second symposium*, edited by H. A. Ernst et al., ASTM STP 1131, Philadelphia, 1992.
- [Raiser et al. 1990] G. Raiser, R. J. Clifton, and M. Ortiz, “A soft-recovery plate impact experiment for studying microcracking in ceramics”, *Mech. Mater.* **10**:1-2 (1990), 43–58.
- [Ravi-Chandar 1995] K. Ravi-Chandar, “On the failure mode transitions in polycarbonate under dynamic mixed-mode loading”, *Int. J. Solids Struct.* **32**:6/7 (1995), 925–938.
- [Ravi-Chandar and Knauss 1984] K. Ravi-Chandar and W. G. Knauss, “An experimental investigation into dynamic fracture, I: crack initiation and arrest”, *Int. J. Fracture* **25**:4 (1984), 247–262.
- [Ravi-Chandar et al. 2000] K. Ravi-Chandar, J. Lu, B. Yang, and Z. Zhu, “Failure mode transitions in polymers under high strain rate loading”, *Int. J. Fracture* **101**:1-2 (2000), 33–72.
- [Ravichandran and Clifton 1989] G. Ravichandran and R. J. Clifton, “Dynamic fracture under plane wave loading”, *Int. J. Fracture* **40**:3 (1989), 157–201.
- [Rosakis et al. 1999] A. J. Rosakis, O. Samudrala, and D. Coker, “Crack faster than the shear wave speed”, *Science* **284**:5418 (1999), 1337–1340.
- [Rosakis et al. 2000] A. J. Rosakis, O. Samudrala, and D. Coker, “Interersonic shear crack growth along weak planes”, *Mater. Res. Innov.* **3**:4 (2000), 236–243.
- [Samudrala et al. 2002] O. Samudrala, H. Huang, and A. J. Rosakis, “Subsonic and intersonic mode, II: crack propagation with a rate-dependent cohesive zone”, *J. Mech. Phys. Solids* **50**:6 (2002), 1231–1268.

[Zhou et al. 1996] M. Zhou, A. J. Rosakis, and G. Ravichandran, “Dynamically propagating shear bands in impact-loaded prenotched plates, I: Experimental investigations of temperature signatures and propagation speed”, *J. Mech. Phys. Solids* **44**:6 (1996), 981–1006.

Received 19 Jun 2006. Revised 30 May 2007. Accepted 31 May 2007.

WEI MA: [watwm@imech.ac.cn](mailto:watwm@imech.ac.cn)

*Institute of Mechanics, Chinese Academy of Sciences, 15 Beisihuanxi Road, Beijing 100080, China*

ZHUPING DUAN: [zpduan@imech.ac.cn](mailto:zpduan@imech.ac.cn).

*Institute of Mechanics, Chinese Academy of Sciences, 15 Beisihuanxi Road, Beijing 100080, China*